Journal of Earthquake Engineering, Vol. 9, No. 2 (2005) 173–197

Imperial College Press
www.icpress.co.uk

AN EVALUATION OF THE STRONG GROUND MOTION RECORDED DURING THE MAY 1, 2003 BINGÖL TURKEY, EARTHQUAKE

SÍNAN AKKAR

Department of Civil Engineering and Disaster Management Center
Middle East Technical University, Ankara, 06531, Turkey

DAVID M. BOORE

US Geological Survey, 345 Middlefield Road
Menlo Park, California 94025, USA

POLAT GÜLKAN

Department of Civil Engineering and Disaster Management Center
Middle East Technical University, Ankara, 06531, Turkey

Received 5 January 2004
Revised 16 August 2004
Accepted 16 August 2004

An important record of ground motion from a **M**6.4 earthquake occurring on May 1, 2003, at epicentral and fault distances of about 12 and 9 km, respectively, was obtained at a station near the city of Bingöl, Turkey. The maximum peak ground values of 0.55 g and 36 cm/s are among the largest ground-motion amplitudes recorded in Turkey. From simulations and comparisons with ground motions from other earthquakes of comparable magnitude, we conclude that the ground motion over a range of frequencies is unusually high. Site response may be responsible for the elevated ground motion, as suggested from analysis of numerous aftershock recordings from the same station. The mainshock motions have some interesting seismological features, including ramps between the P- and S-wave that are probably due to near- and intermediate-field elastic motions and strong polarisation oriented at about 39 degrees to the fault (and therefore not in the fault-normal direction). Simulations of motions from an extended rupture explain these features. The N10E component shows a high-amplitude spectral acceleration at a period of 0.15 seconds resulting in a site specific design spectrum that significantly overestimates the actual strength and displacement demands of the record. The pulse signal in the N10E component affects the inelastic spectral displacement and increases the inelastic displacement demand with respect to elastic demand for very long periods.

Keywords: Bingöl earthquake of May 1, 2003; site amplification; wave propagation/ polarisation; design spectrum; inelastic displacement demand.

1. Introduction

The city of Bingöl in eastern Turkey was struck by a **M**6.4 earthquake on May 1, 2003 at 03:27 local time (01:27 GMT). Seven strong motion stations were triggered during the mainshock of the Bingöl earthquake. Among these, the ground

motions recorded by six stations (Tercan, Erzincan, Elazığ, Muş, Tatvan, and Kahramanmaraş) have peak ground acceleration (PGA) values of less than $0.01\,g$ due to their large distances from the source. The Bingöl station was closest to the mainshock with epicentral and fault distances of about 12 and 9 km, respectively, and the two horizontal and vertical PGA values recorded were $0.55\,g$, $0.28\,g$ and $0.47\,g$, respectively. The $0.55\,g$ horizontal PGA is among the largest ground acceleration peaks recorded in Turkey, and its seismological features and its effects on structures deserve to be scrutinised further.

2. Tectonic Information

The epicenter of the mainshock was located to the north of Bingöl, a city that is surrounded by a set of very complex and heterogeneous faults as indicated by the regional seismotectonics in Fig. 1. The earthquake occurred inside the

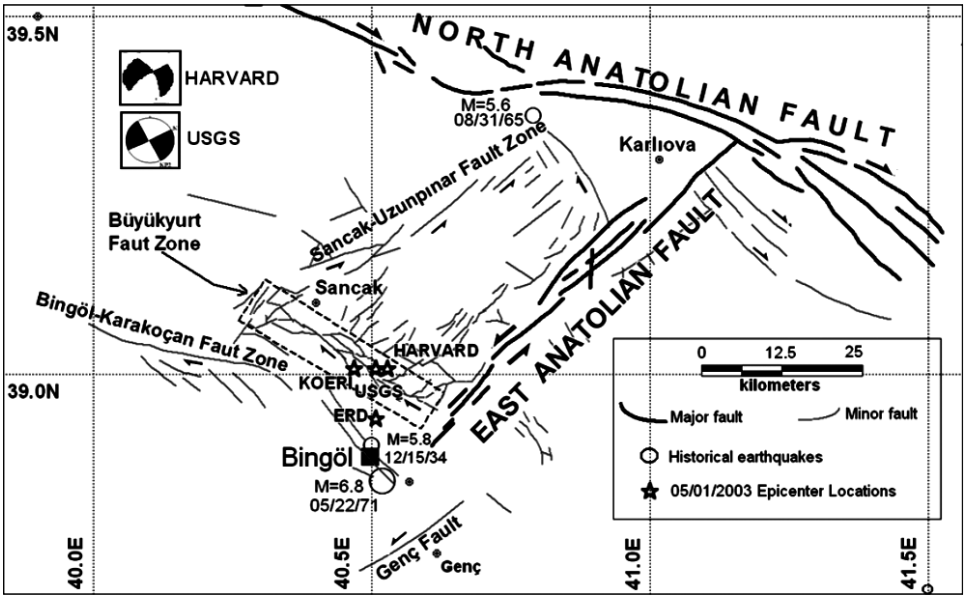

Fig. 1. Simplified overview of the most important faults and historically important earthquakes in the region. The strike-slip North Anatolian and East Anatolian faults run in the Northwest-Southeast and Northeast-Southwest directions, respectively. The minor faults inside the Bingöl-Erzincan-Karlıova triangle extend from these two major faults. The strike-slip faults that are parallel to North Anatolian fault are right lateral, whereas the strike-slip faults parallel to East Anatolian fault are left lateral. The map also shows the epicentre locations and fault plane solutions reported by various agencies. (The USGS and Harvard report the centroid location of the earthquakes.) The CMT solution of Harvard describes a non-double couple component indicating a complex faulting (http://www.seismology.harvard.edu). The right lateral strike-slip Büyükyurt fault zone was reported as ruptured during the Bingöl earthquake [Koçyiğit and Kaymakçı, 2003]. The recording station is approximately 9 km south of Büyükyurt fault zone indicated by the rectangular block. (Abbreviations: USGS is the United States Geological Survey; HARVARD is the Harvard Seismology Laboratory at Harvard University; KOERI is the Kandilli Observatory and Earthquake Research Institute of Boğaziçi University; ERD is the Earthquake Research Department of the General Directorate of the Disaster Affairs, Turkey.)

Bingöl-Karlıova-Erzincan triangle that is defined by the Karlıova triple junction to the east, the right lateral strike-slip North Anatolian fault (NAF) to the north and left lateral strike-slip East Anatolian fault (EAF) to the south. The Bingöl-Karlıova-Erzincan triangle is traversed by conjugate faults of the NAF and the EAF that run in the NE-SW and the NW-SE directions, respectively. The left lateral strike-slip conjugate faults extend from the NAF and follow a parallel pattern to the EAF (i.e. NE-SW direction). The right lateral strike-slip conjugate faults extend from the EAF and follow a pattern parallel to the NAF (i.e. NW-SE direction). These faults do not follow a straight path but define an *en echelon* pattern. The 1784 Yedisu and 1866 Göynük-Karlıova earthquakes were the most devastating earthquakes experienced in the province of Bingöl [Ambraseys, 1988]. The last damaging earthquake before this recent event was the May 22, 1971 Bingöl earthquake ($M_s = 6.8$) that was nucleated on the EAF, approximately 10 km to the south of the city [Ambraseys and Jackson, 1998]. Reflecting on the seismicity of the Bingöl-Karlıova-Erzincan triangle from different authors [Ambraseys, 1988; Ambraseys and Jackson, 1998; Seymen and Aydın, 1972] the May 1 event can be considered a medium size earthquake that could be expected to occur frequently within the faulting system described above.

Koçyiğit and Kaymakçı [2003] reported clear traces of surface rupture on the right lateral strike-slip Büyükyurt fault zone (with a strike of 115 degrees) that correlates well with the reported epicentres by various agencies, as shown in Fig. 1. The focal mechanism solutions of the USGS and Harvard-CMT indicate a strike of 154 and 152 degrees, respectively, for the right lateral strike-slip fault plane. The difference in strike angle between what can be inferred from the geological data and the focal mechanism solutions of the USGS and the Harvard-CMT is 39 and 37 degrees, respectively. Focal mechanism calculations would not normally have that much error even with the uncertainties that are overlooked in the solutions (Stuart A. Sipkin, personal communication). We note that there are contradictory comments about the surface rupture of the Bingöl earthquake. Koçyiğit and Kaymakçı [2003] is the only source to report a visible surface rupture from geological observations. Other geological research teams in the earthquake area did not report the existence of surface rupture [Emre *et al.*, 2003; personal communication with the NSF geological team that visited the earthquake area].

A recent study by Li *et al.* [2004] used locations of aftershocks recorded on an array installed by ERD (agency who owns the national network recording stations and is responsible for the dissemination of the raw data) after the mainshock to estimate the geometry of the mainshock rupture surface. The best fitting single rupture plane has a strike of 141 degrees, but Li *et al.*'s preferred rupture geometry consists of two planes, with the northwesterly plane striking 135 degrees, abutting at about 5 km northwest of the epicentre with a plane striking 155 degrees. Our paper does not depend critically on the strike of the fault planes, and for purposes of analysis in this paper, we assume that the faulting took place on the Büyükyurt fault zone, with a strike of 141 degrees clockwise from north. This strike is a compromise between the report of surface faulting, the focal mechanism solutions, and the results

of Li *et al.* [2004]. The depth of the Bingöl earthquake was reported as 10 km by USGS. The location information given by Harvard-CMT computed the depth as 15 km.

3. Information on Acceleration Sensor and Recording Station

The strong ground motion instrument deployed in the Bingöl station is a ±2 g-limit force-balanced, tri-axial accelerometer (SSA-320 by Terra Technology Corp.[a]) with a natural frequency of 50 Hz and a critical damping ratio of 0.7 as default factory settings. The accelerometer response approximates a second-order system that is fairly flat in amplitude for frequencies below the natural frequency. Above the natural frequency the response is asymptotic to 12 dB per octave. The data acquisition system is a 16-bit analog-to-digital recorder (GSR-16 GeoSys AG[b]) that was set to have a pre-event memory of 20 seconds and a sampling rate of 100 Hz at the time of the earthquake.[c]

The drawing in Fig. 2 shows the general view of the Bingöl recording station. This is a reinforced concrete office complex of the Bingöl Public Works and Settlement Directorate. The strong ground-motion instrument is placed inside the one-storey appurtenant structure that is adjacent to the mid-rise office buildings. Expansion joints separate each adjacent block in the complex. The buildings have

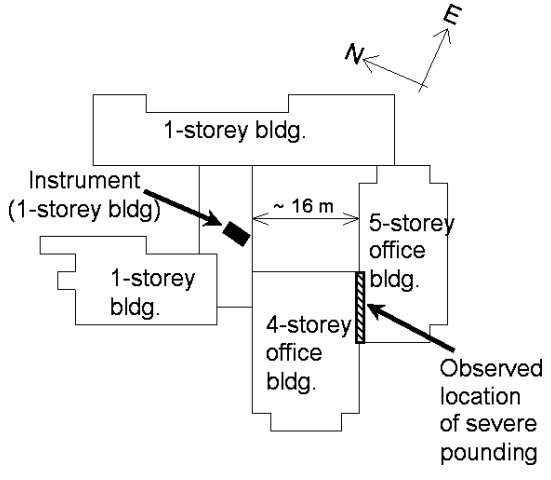

Fig. 2. Bingöl Public Works and Settlement branch office complex, which includes the 5-storey reinforced concrete main office building connected to a 4-storey office building with a 1-storey building containing the accelerometer sensor approximately 16 m from the 4- and 5-storey buildings. The two mid-rise buildings experienced pounding in the NS direction during the main event.

[a]Terra Technology Corp. Redmond, Washington 98052 USA.
[b]GeoSys AG Kanalstrasse 11 8152 Glattbrugg Switzerland.
[c]Trade, product, or firm names are for descriptive purposes only and do not imply endorsement by the US Government or other entity.

been designed and constructed according to template designs developed by the parent Ministry. Identical provincial Public Works and Settlement building complexes exist in many cities of the country. As a comment of interest, we note that similar building complexes in Erzincan, Bolu, and Bingöl have experienced strong shaking from earthquakes in 1992 (Erzincan), 1999 (Düzce), and 2003 (Bingöl). The Bingöl station is located in the north of the city, on a terrace between two streams incised about 50 m beneath the terrace level. The stiff terrace materials contain rounded and semi-rounded blocks in a clay matrix. The terrace deposits rest on volcanic rocks. Shear-wave velocities obtained from a seismic refraction survey at the site (Gürbüz and Çeken, personal communication, 2003) are relatively high, with an average velocity over the upper 30 m of 806 m/sec, making this a NEHRP class B site (760 m/sec $< V_{S(30)} <$ 1500 m/sec).

Figure 3 shows a photograph of the recording instrument. The sensor is placed on a reinforced concrete pedestal in one of the storage rooms of the one-storey appurtenant building. The pedestal is inside a 0.5 m deep, 1.0 m by 1.0 m excavation to minimise interaction between the structure and the sensor. As shown in the cross-section drawing, the pedestal extends to a depth of 2.0 m. This figure also shows the directions of the principal axes of the tri-axial sensor. As there has been some dispute regarding the orientation of the sensor, we have made a special effort to determine the correct orientation. The orientation shown in Fig. 3 differs by 10 degrees from that reported by the ERD. Our sensor orientation is based on

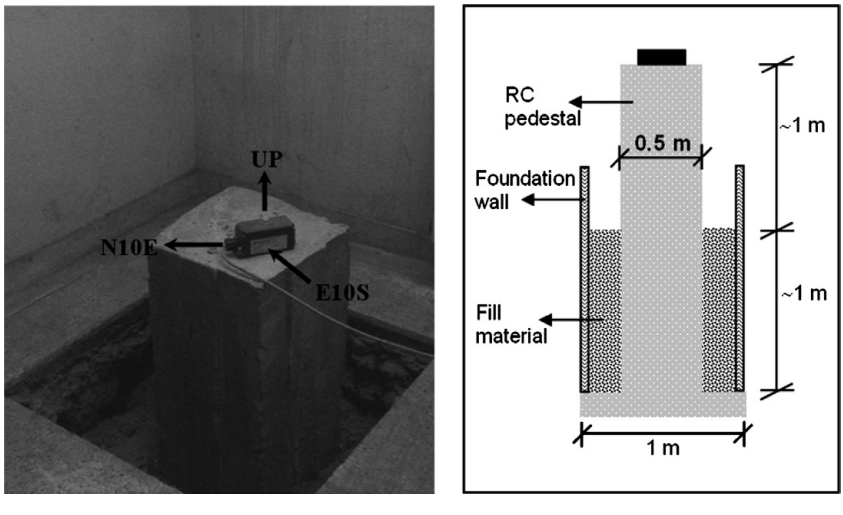

Fig. 3. The deployment of sensor in the Bingöl station and the directions of the principal axes. The instrument is placed on a reinforced concrete pedestal inside a 1×1 m foundation to minimise the interaction between the structure and the sensor. The square pedestal cross section is 0.5×0.5 m and its height over the surface is approximately 1.0 m. The pedestal is embedded approximately 1.0 m beneath the surface. The sensor orientations account for the influence of the metal case and electric fields from the sensor. The orientations differ 10 degrees from those reported by ERD on their web site (http://angora.deprem.gov.tr/).

measurements made by the NSF team and includes a correction for the influence of the metal case and the electric fields from the sensor.

4. Ground Acceleration, Velocity and Displacement

The acceleration traces as recorded are shown in Fig. 4, and Fig. 5 shows the integrated velocity and displacement traces from the horizontal component acceleration records, computed by removing the pre-event mean of the first 18 seconds from the raw data. We call this process the zeroth-order correction. The long pre-event motion permitted us to compute the pre-event mean with confidence, and the lack of any drifts of the pre-event zero line in the velocity and displacement traces indicates that the baseline is stable in the pre-event portion of the record. This is not the case later in the motion, however; the integrated raw velocity time series shows a linearly increasing trend that translates to a quadratic trend in the displacement traces. Thus, a baseline correction is required to obtain a more reliable picture of the particle motion for the mainshock. Of the numerous baseline correction procedures, the results of only two alternative methods will be discussed here. The first trial (Alternative 1) simply fits a straight line to the final portion of the raw velocity data where the ground motion is about to cease. This velocity line is extended to a time t_2, and another straight line connects that time to a time t_1 at the start of the record. This procedure is a modified version of the data processing

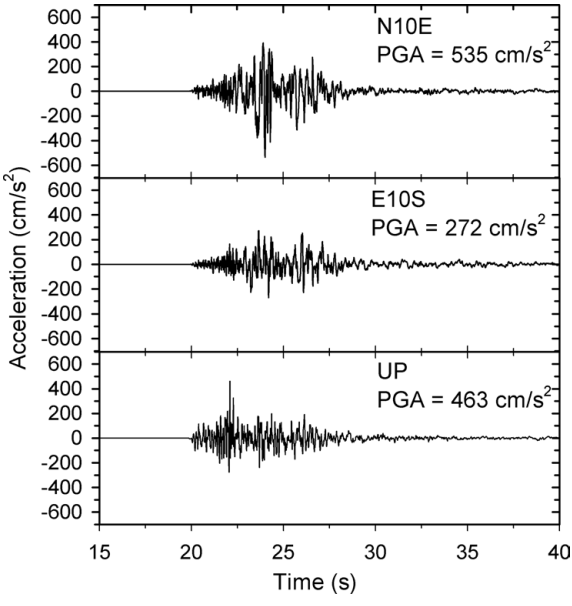

Fig. 4. The acceleration traces recorded by the Bingöl station. This information has been released by the Earthquake Research Division of the General Directorate of Disaster Affairs. The times shown on the abscissa are relative to the start of the recording, which includes a 20 seconds pre-event buffer (not all of the buffered motion is shown).

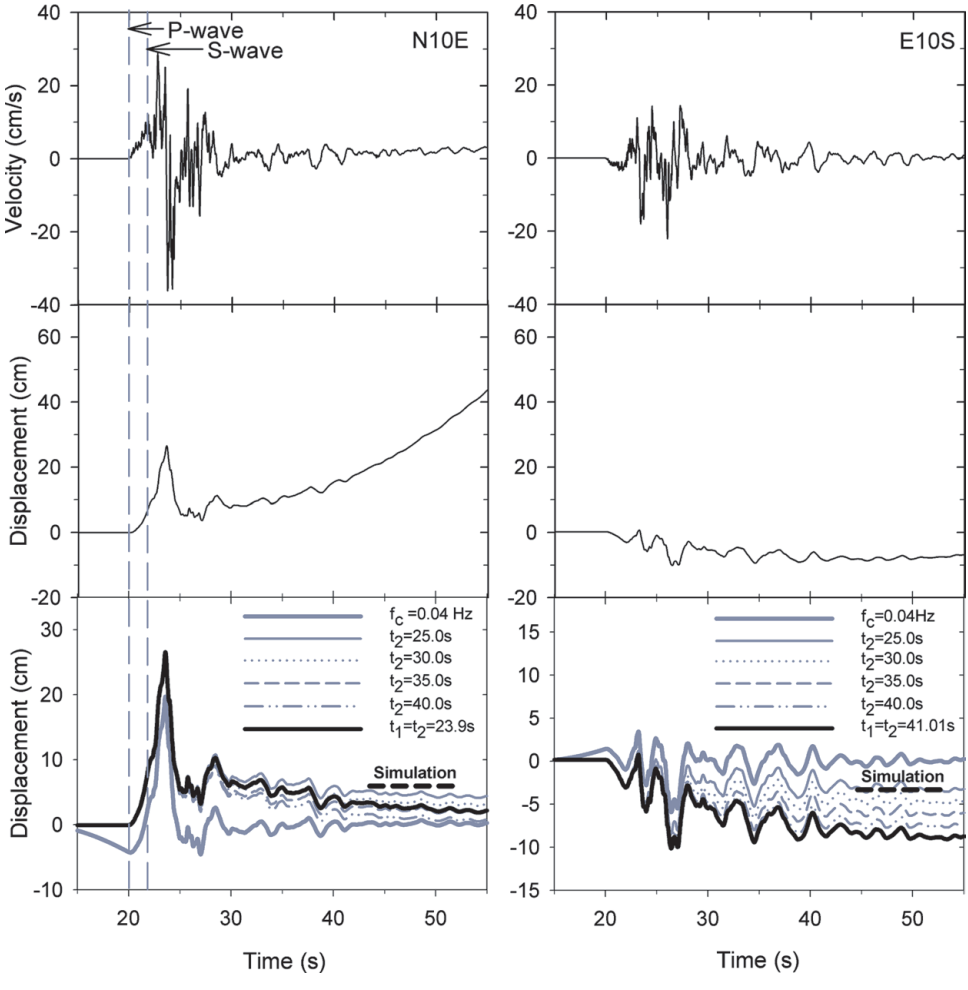

Fig. 5. The first two rows show the velocity and displacement traces for the horizontal components obtained from integration after removing the mean of the first 18 seconds from the complete acceleration records. The third row shows the comparisons of the ground displacements derived using alternative baseline correction methods. The dark, thicker grey line is the resultant displacement obtained by removing the long-period components of motion by acausal Butterworth filtering, with a corner frequency of 0.04 Hz and a filter order chosen so that the filter response goes as f^4 at low frequencies. The time series were padded with 20 and 40 seconds of leading and trailing zeros before filtering to account for the impulse response of the filter; these padded sections were removed in the plots shown here. The rest of the curves are doubly integrated displacement time series using the modified versions of the scheme proposed by Iwan *et al.* [1985]. In all cases, the nonphysical drift in the uncorrected ground velocity is removed by fitting straight lines to the uncorrected velocity traces. The slopes of the straight lines are used to remove the steps in the acceleration. The black thick line shows the resultant displacement time series of the correction method selected for this study. Note that the ordinate scales are different for the two components.

scheme proposed by Iwan *et al.* [1985] and described in detail by Boore [2001] and by Boore *et al.* [2002]. The task is to choose the times t_1 and t_2. We fix t_1 at the start of the record. The simplest way to determine t_2 is to let it be the time at which the fitted velocity line intersects zero (for this case, the choice of t_1 is immaterial, we indicate $t_1 = t_2$ in the figure to indicate this simplest procedure). We show results using this choice of t_2 as well as a series of other choices. The residual displacements vary widely, but they have the direction and general amplitude expected from a model of finite faulting in an layered elastic medium. The second correction process (Alternative 2) is the filtering of raw acceleration data. We used a low order acausal Butterworth filter with a corner frequency (f_c) of 0.04 Hz. Acausal filters do not have phase distortions that result in diminished sensitivity of elastic and inelastic response spectra to the filter cut-off frequencies [Boore and Akkar, 2003]. Note that leading and trailing zeros are required for acausal filters, and this is achieved by using the procedure suggested by Converse and Brady [1992]. The leading and trailing zeros for the filtered data are excluded from the corrected traces in order to facilitate observing the differences between the various correction procedures. As expected, the displacement derived from the filtered acceleration oscillates about zero late in the record. The precursory motion of the displacements that are derived from filtering is due to the acausal filter transient. The peak amplitude of the signal in N10E component is diminished by the low-cut filtering, but the peak-to-trough displacements are nearly the same for all correction procedures. The precursory motions resulting from zero padding may lead to possible misinterpretation in the discussions on ground motion polarization. Thus, we will use the ground motions corrected by Alternative 1 with $t_1 = t_2$ for the rest of this article. The velocity and acceleration traces for all of the processing schemes are virtually indistinguishable.

5. Seismological Aspects of the Ground Motion Data

We discuss here the characteristics of the horizontal ground motions recorded at Bingöl, focusing particularly on the large motions on the N10E component. The ground motion exhibits near- and intermediate-field contributions and is strongly polarised. The overall level of the motion significantly exceeds motions expected for an earthquake of this magnitude. There are a number of possible reasons for this large motion, including directivity and site response. We think that site response, in particular, had a significant influence on the peak acceleration.

5.1. *Ramp in velocity and displacement*

By enlarging the velocity plots in Fig. 5, it is possible to pick the initial P- and S-wave arrivals at 19.9 and 21.85 seconds, respectively (we interpret the down turn in velocity on the N10E component to correspond to the initial S-wave arrival). The time difference of 2.0 seconds is consistent with a hypocentral distance of about 14 km, in general agreement with the epicentres shown in Fig. 1 and with the shallow

focal depth solutions of USGS and Harvard-CMT. What is remarkable, however, are the ramps in velocity and displacement between the P and the S arrivals (Fig. 5). At first we thought these were artifacts due to unstable acceleration baselines, but after considering a number of methods for baseline correction, and primarily as a result of comparisons with synthetic seismograms (to be shown shortly), we think that the ramps are real and are due to the near- and intermediate-field terms in the elastic wave motion.

5.2. *Polarization of motion*

The velocity and, in particular, the displacement ground motions shown in Fig. 5 indicate a strong polarisation. To better see this, we combined the two horizontal components into hodograms, as shown in Fig. 6. The hodograms are shown for the main pulse of motion between 20 and 25 seconds, and all three types of motions — acceleration, velocity, and displacement — show a polarisation in the north-south direction. This is more-or-less the perpendicular direction to the cluster of epicentres shown in Fig. 1, and is about 39 degrees from the fault strike. If the dominant motion had originated on the portion of the fault near the epicentre, we would have thought that the predominate S-wave motion from a vertical strike-slip fault would be oriented transverse to the direction of wave propagation, and thus we expected the S-wave motion to be polarised in a more east-west direction than the observed polarisation. We made sense of the observed orientation only after comparing the observed motions to those from synthetic seismograms from an extended rupture. The synthetic motions were provided by R. Graves, and although not intended to model the Bingöl motions, they were computed for a geometry similar to that corresponding to the Bingöl situation. We judge that the simulations can provide a semi-quantitative comparison with the data. The synthetics were for a magnitude 6.5 vertical strike-slip fault in a layered crust and assumed a randomly-generated slip distribution with a hypocentre that would correspond to a point somewhat to

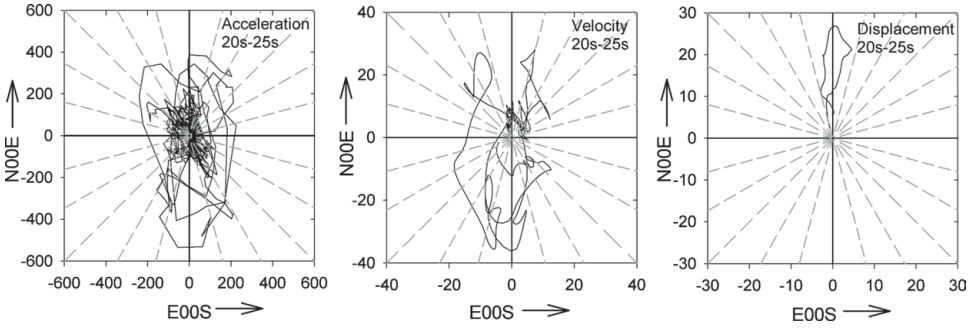

Fig. 6. Hodograms of the horizontal motions. The plots are drawn for the time interval that brackets the strong ground motion phase of the records. The dashed light lines are drawn at every 15 degrees.

the NW of the epicentres shown in Fig. 1; the particular slip distribution for the synthetics shown here was relatively concentrated near the assumed hypocentre. The comparisons of the observed and simulated traces are shown in Fig. 7. The observed motions were rotated into fault parallel and fault normal directions assuming a fault strike of 141 degrees (a choice discussed in Sec. 2). Because the simulations did not include high frequencies, we applied a high-cut filter with a corner frequency at 0.5 Hz to the observations. Figure 7 shows that the ramp in motion between the P- and S-wave arrivals exists in the simulations and that the polarisations of the simulations and the observations are similar for a slip motion concentrated near the hypocentre. Furthermore, the model results suggest that SV waves are an important

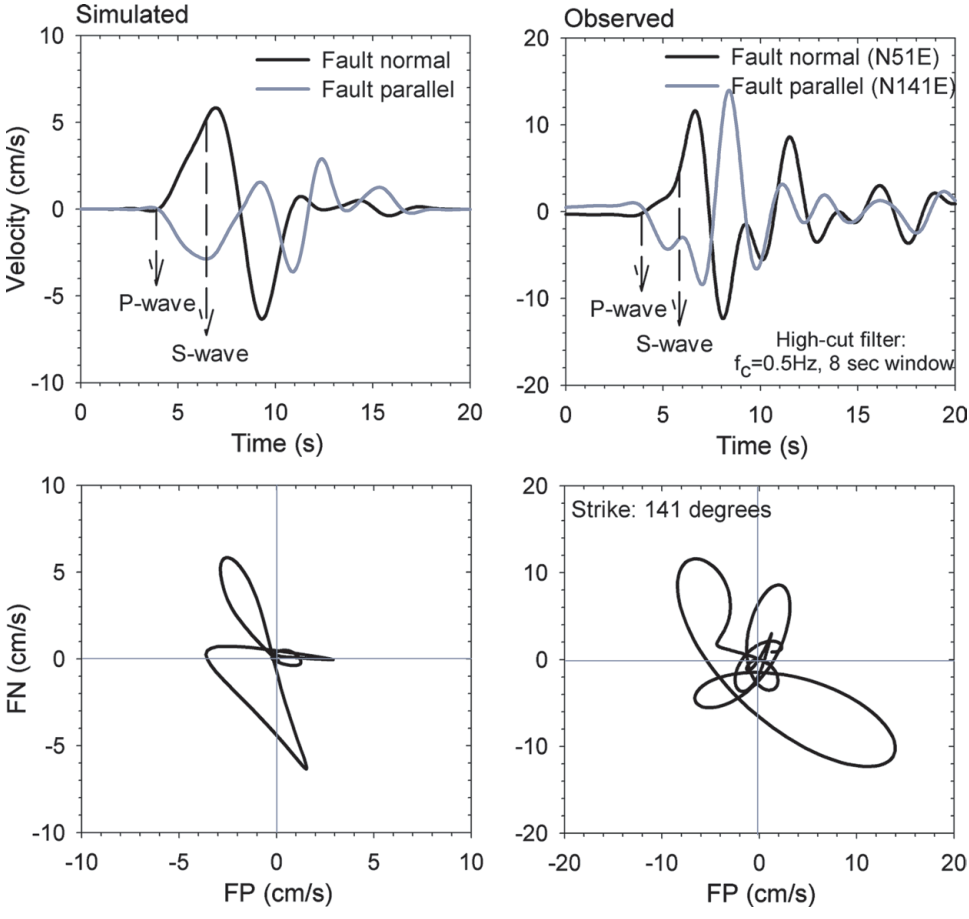

Fig. 7. Simulated and observed velocities and related hodograms. The observed time series and hodograms are rotated into fault normal and fault parallel directions assuming a fault strike of 141 degrees (see text). The dashed arrows show the estimated P- and S-wave arrivals according to the layered velocity model and slip distribution along the fault. (Time scale in the simulated velocities are different than the scaling in Figs. 4 and 5 for convenience. The arrival times of P- and S-wave phases are consistent with the ones shown in Fig. 5.)

contributor to the motion recorded at the Bingöl station. Thus, we think that the features in the observations that we at first took to be peculiar are in fact natural consequences of the fault-station geometry and the proximity of the station to the fault.

It is clear from the hodogram of the data in Fig. 7 that the polarisation is not a maximum in the fault normal direction, as has been suggested by some researchers [e.g. Somerville *et al.*, 1997]. The difference between the actual NS direction of polarisation for the observed data and the fault normal would have been even larger if we had used Li *et al.*'s [2004] two-segment fault surface, in which case the plane closest to the Bingöl station has a strike of 155 degrees. The fault normal for that plane differs from the direction of observed polarisation by 65 degrees. Other studies have also found that the peak near fault motions are not necessarily in the fault normal direction [Akkar and Gülkan, 2002; Howard *et al.*, 2003].

5.3. *Large ground motions*

The peak acceleration from the Bingöl record is unusually large. There are various ways to show this but our conclusion is based primarily on the comparison of peak accelerations to those predicted using data from other earthquakes. The equations of Abrahamson and Silva [1997], Ambraseys and Douglas [2002], Boore *et al.* [1997], Campbell [1997, 2000], Gülkan and Kalkan [2002], and Sadigh *et al.* [1997] yield median PGA values ranging between $0.18\,g$ and $0.29\,g$ for a fault distance of about 9 km. The 84th percentiles range between $0.28\,g$ and $0.49\,g$ for the same distance (the PGA values have been adjusted for differences in site response between the average rock site for the equations above and the Bingöl site by using the factors of Boore *et al.*, 1997, with a 30 m average shear-wave velocity in the equations of 520 m/sec (W. Silva, personal communication)). The observed motion of $0.55\,g$ is well above the 84th percentile predictions. It is not just the peak acceleration that is high — the response spectra over a wide range of periods are larger than median motions from prediction equations, with the spectrum for the N10E component exceeding the 84th percentile for periods surrounding large peaks at 0.15 seconds and 0.6 seconds (Fig. 8, with graphs using both log and linear scales to help in comparing observed and predicted motions). The spectra in Fig. 8 from the ground-motion prediction equations represent the motion from an average source, path, and site, with all complications smoothed out (for example, the site amplifications do not account for local site resonances). Thus we can take the deviations from the predicted motions shown in Fig. 8 as an indication of source, path, or site complexity. The difficulty is in distributing the complexity amongst the various possibilities.

Why are the motions so large, particularly for the N10E component? Many factors can play a simultaneous role in enhancing motion, and it is well-known that ground motion has significant variability that is not easy to assign to a single cause [e.g. Boore, 2004]. We discuss several possibilities here, with an emphasis on

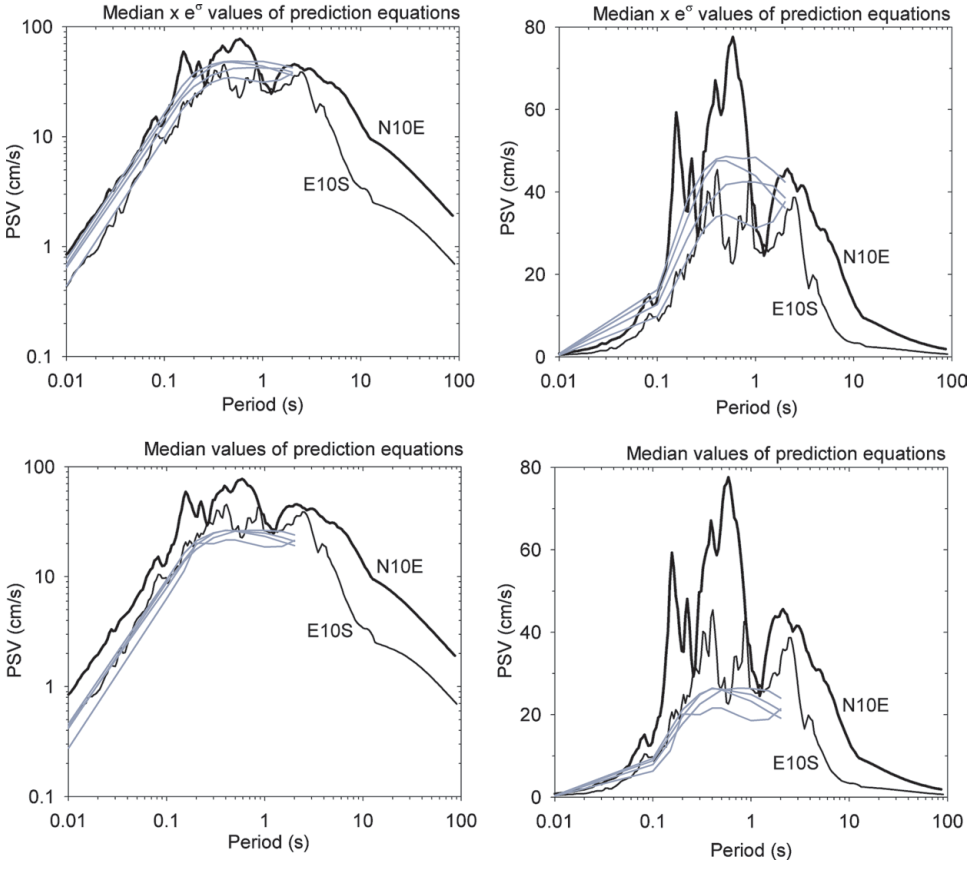

Fig. 8. Comparisons of observed and predicted pesudo-velocity spectra. The predictions from Boore *et al.* [1997], Campbell [1997, 2000], Sadigh *et al.* [1997], and Abrahamson and Silva [1997] are plotted in grey.The prediction equations consider the shear-wave velocity for an average rock site. The straight lines in the plots of predicted spectra between 0.01 seconds and 0.1 seconds are artificial; they connect the value of PGA, assigned to a period of 0.01 seconds, and the predicted values of the response spectra at 0.1 seconds.

the peak acceleration. The peak acceleration is strongly related to a large, narrow-band peak in the Fourier amplitude spectrum, centered at 6.5 Hz (Fig. 9). Wen *et al.* [2001] concluded that a concrete pedestal on which the instrument was mounted amplified peak accelerations, thus producing a 1.0 g recording obtained at a station during the 1999 Chi-Chi, Taiwan earthquake. The sensor that recorded the Chi-Chi earthquake was mounted on a more massive pedestal than the one on which the Bingöl earthquake was recorded (for Chi-Chi, a 3.0 m long, 1.0×1.0 m concrete column embedded in the earth; for Bingöl, a 2.0 m long, 0.5×0.5 m column (Fig. 3)). Our careful reading of Wen *et al.* [2001], along with calculations of the Fourier spectra of the motions at the Chi-Chi station, suggests that only part of the amplified motion is due to the resonance of the column. To get a rough idea of the effect of a

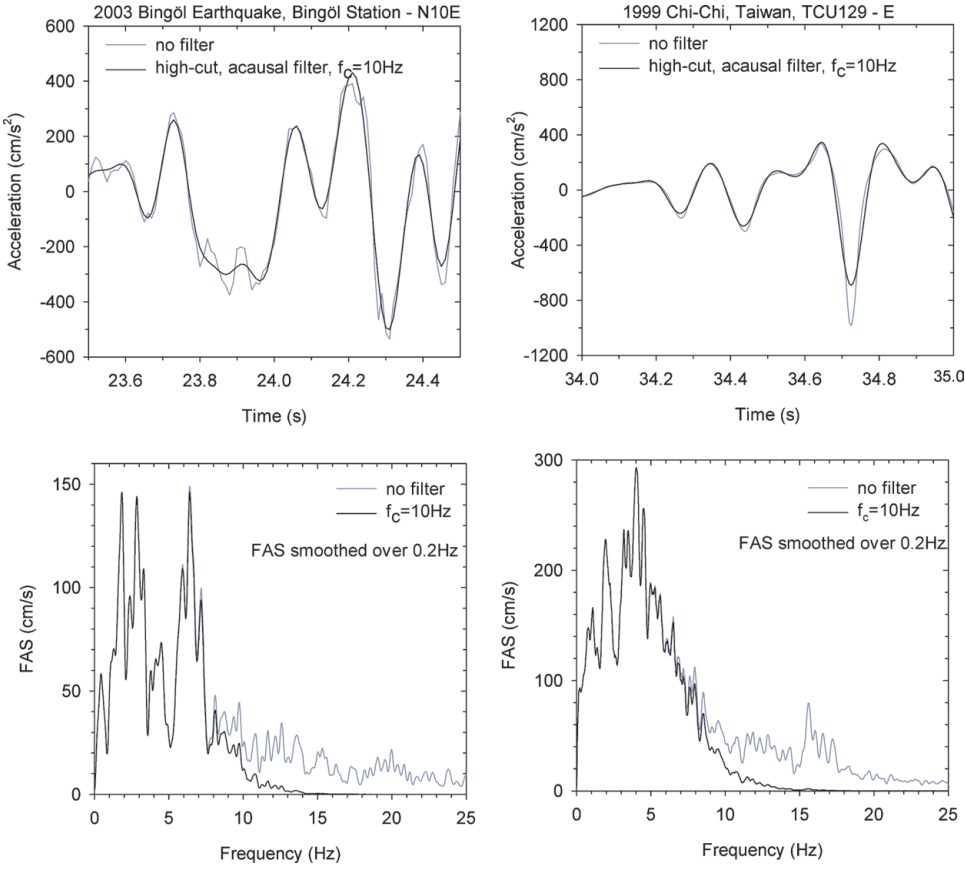

Fig. 9. Unfiltered and filtered acceleration time series for the Bingöl N10E and Chi-Chi TCU129 E records. The filter corner frequency is 10 Hz in both cases. The second row shows the corresponding Fourier amplitude spectra. The pedestal resonance is effective at 20 Hz and 16 Hz for the Bingöl N10E and TCU129 E records, respectively. The TCU129 peak acceleration is affected by frequencies above 10 Hz.

column, we calculated the resonant frequency of a 2.0 m high cantilever beam with cross-sectional area and material properties consistent with the Bingöl station using an equation in Clough and Penzien [1993, p. 382]. The result was 40 Hz. Inspection of the Fourier spectra for both the Chi-Chi and the Bingöl records (Fig. 9) show a narrow-band amplification in the spectra around 20 Hz and 16 Hz for Bingöl and Chi-Chi, respectively. We suggest that these are related to the column response. To see the effect of these amplifications on the peak accelerations, we applied high-cut filters with a corner at 10 Hz. The results, shown in Fig. 9, indicate that the Chi-Chi peak acceleration is somewhat affected by the motion above 10 Hz, in contrast to the peak acceleration for the Bingöl recording. On this basis, we conclude that the column on which the sensor was mounted did not affect the peak acceleration of the Bingöl recording.

Severe pounding between the two mid-rise office buildings was observed immediately after the mainshock; the location of this pounding is indicated in Fig. 2. Similar pounding was observed on the same type of buildings at Bolu during the 12 November 1999 Düzce **M**7.2 earthquake (with a peak acceleration of $0.82\,g$). Both peaks on the acceleration traces appear to be short duration. Is it just a coincidence that the large peak accelerations also occurred near buildings that pounded against one another, or are the large peak accelerations a result of the pounding? It is hard to come to a conclusion one way or another without a detailed analysis of the amplitude and frequency content expected from the pounding of buildings, so we leave this possibility as a conjecture, and will not pursue it further.

It is well known that fault rupture toward a station can enhance ground motions (an effect termed "directivity"). This has been used as an explanation for large motions near the Aigio earthquake in Greece with a magnitude similar to the Bingöl earthquake [Lekidis *et al.*, 1999]. Although directivity probably played a part in enhancing the Bingöl motions, we think it was not the only important factor. Unlike the Bingöl earthquake, the Aigio earthquake apparently ruptured directly toward the recording station, thus maximizing the directivity effect. The enhanced motions at relatively short periods might also be used to argue against the importance of directivity, as Somerville *et al.* [1997, with a revision by Abrahamson, 2000] find that directivity is only important for periods exceeding 0.6 seconds. But Boatwright and Boore [1982] found clear evidence that peak acceleration can be strongly influenced by directivity.

Another possible mechanism for enhancing the ground motions is local site amplification. We discuss this in some detail. We computed site amplifications for the shear-wave velocity model provided by Gürbüz and Çeken (personal communication, 2003), assuming three angles of incidence. The results are shown in Fig. 10. As we are primarily interested in the frequencies of peak amplification, no damping was included in the calculations. The amplification is relative to the shallow half space at 20 m depth. The calculations indicate a resonance around 10 Hz. It is possible that the observed spectral peak at 6.5 Hz is a result of site resonance, particularly if nonlinear response shifts the resonance frequency to lower frequencies, and if the variability between observed and calculated site resonances in other studies is considered [Boore, 2004].

If the high-amplitude, narrow spectral peak at 6.5 Hz were due to site response rather than building pounding or source complexity, we would expect to see it on aftershock records. To investigate this possibility, we computed Fourier spectra for 59 aftershock time series obtained from the same instrument that recorded the mainshock. All aftershock records have PGA values of less than $0.01\,g$, magnitudes in the range $3.0 \leq \mathbf{M} \leq 4.2$, and epicentral distances, R, in the range $5\,\text{km} \leq R \leq 31\,\text{km}$. (The agency in charge of the aftershock records gives the duration magnitudes, M_d for the aftershock data. For further computational purposes, we converted the M_d to **M** by using the relationship derived by Bakun [1984]. The conversion changed the M_d values at most by a multiplicative factor of between

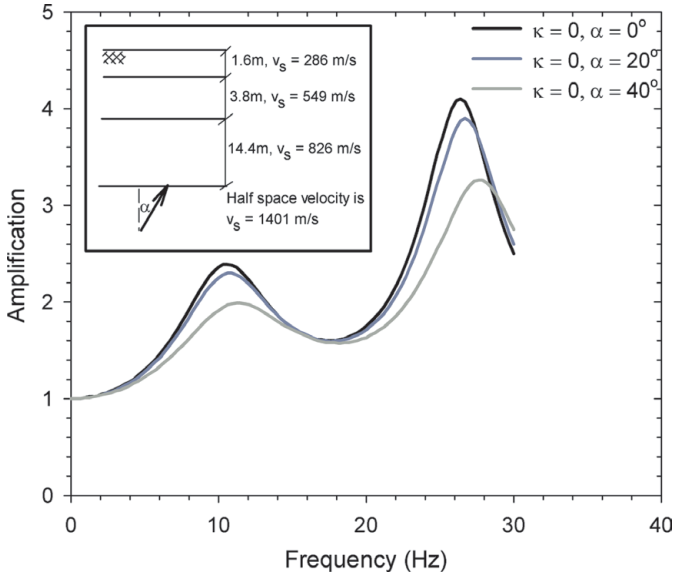

Fig. 10. Velocity model and site amplification for the recording station. The computations are done for waves propagating in three different incident angles: 0, 20, and 40 degrees. The small figure on the upper left side shows the soil layer thicknesses and shear-wave velocities provided by Mustafa Gürbüz and Ulubey Çeken from ERD.

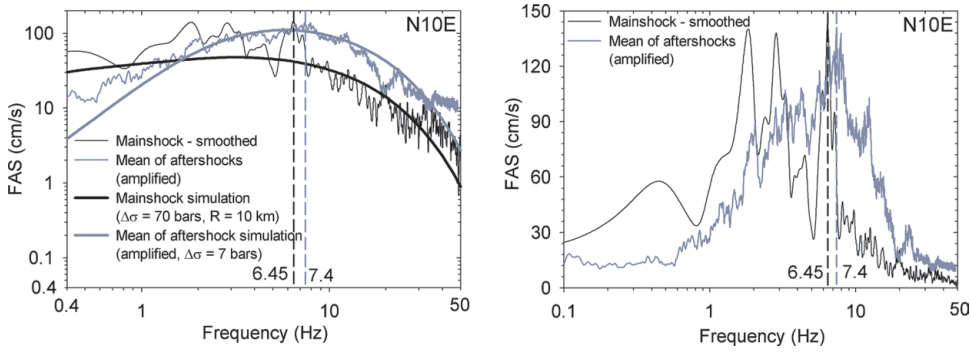

Fig. 11. Fourier amplitude spectrum of the mainshock (black line) and arithmetic mean of 59 aftershocks (grey line). The mean aftershock spectrum has been normalised so that its maximum amplitude equals that of the mainshock. The mainshock Fourier amplitudes were smoothed with a Parzen's lag window with a bandwidth of 0.4 Hz. Included in the plot on the left are simulations for the mainshock and for an average aftershock. The spectrum for the aftershock simulation has been normalised by the same factor used to normalise the spectrum for the aftershock data.

0.94 and 1.01. The duration magnitudes reported by the agency range between 3.0 and 4.5). We focused on the N10E component of the motion in pursuit of explaining the high-amplification spectral amplitudes on that component during the mainshock. We compare the average spectra from the 59 aftershock records to the mainshock spectrum, for the N10E component, in Fig. 11, again using log and

linear scaling for the ordinate to help judge the comparison of the various curves. For purposes of comparing the shapes, the aftershock spectra have been amplified to equal the peak spectral amplitude of the mainshock motion. Also shown in Fig. 11 are simulated Fourier spectral amplitudes from the stochastic method of Boore [2003], for two values of the stress parameter (and site amplifications for $V_{S(30)} =$ 806 m/sec, using adjustments of the Boore and Joyner [1997] generic amplifications based on the velocity dependence given by Boore *et al.* [1997]). The simulations are shown to provide "base" spectral shapes that account for difference in average ground-motion spectra for the mainshock and the much smaller aftershocks.

Because of the interaction of source corner frequency and local attenuation, the simulated aftershock spectrum have a broad peak in the frequency range within which the narrow-band spectral amplification occurs. Any local site response will appear as local amplifications riding on the broader peak. The mean aftershock spectrum has a local spectral peak at 7.4 Hz, which is slightly higher frequency than the 6.45 Hz spectral peak for the mainshock. We also note that the spectrum in Fig. 11 contains a number of peaks; although it is dangerous to single out just one of them, the ones at 6.45 and 7.4 Hz are the most prominent peaks in the spectra and probably strongly control the peak accelerations. If a site effect, the difference in peak frequencies for the mainshock and the mean aftershock could be due to nonlinear soil response. Of course, the spectral peaks could also be due to source or path effects, and the similarity in frequency could be a coincidence. If the peak frequency changes with earthquake location, which is not at all unusual, then averaging over many events should smooth out any sharp spectral peaks due to non-local effects, unless all the aftershocks occur in the same location.

Yet another way to look for site response, advocated by Çelebi [2003], is to study the ratio of spectra obtained from an upper storey of a structure and the ground level. Peak spectral amplitudes carried by the ground motion should cancel out when the ratio is taken. Luckily, motions from the top floor of the largest building in the Bingöl recording station complex were obtained for aftershocks on an instrument installed after the mainshock. The ground floor recordings are those obtained from the same instrument that recorded the mainshock. The accelerations, smoothed Fourier amplitude spectra, and ratios of smoothed spectra are shown in Fig. 12 for three aftershocks. For all of the aftershocks there is a clear amplification near 2.0 Hz, and the somewhat jagged ratios at higher frequencies suggest amplifications at 6.0–7.0 Hz and 10 Hz. The amplification near 2.0 Hz is undoubtedly the five-storey building resonance, and the other two resonances are at the classical multiples of 1:3:5, so they probably represent the first and second higher modes of the structure. To signify site response, however, we need to see spectral peaks in the individual spectra that are eliminated in the ratio. The clearest example of this is for the **M**4.3 aftershock (left panel of Fig. 12), which have prominent spectral peaks at frequencies at about 4.5, 5.5, 7.5 Hz in both the top storey and the ground floor records. These peaks cancel out in the ratio and so are probably being carried in

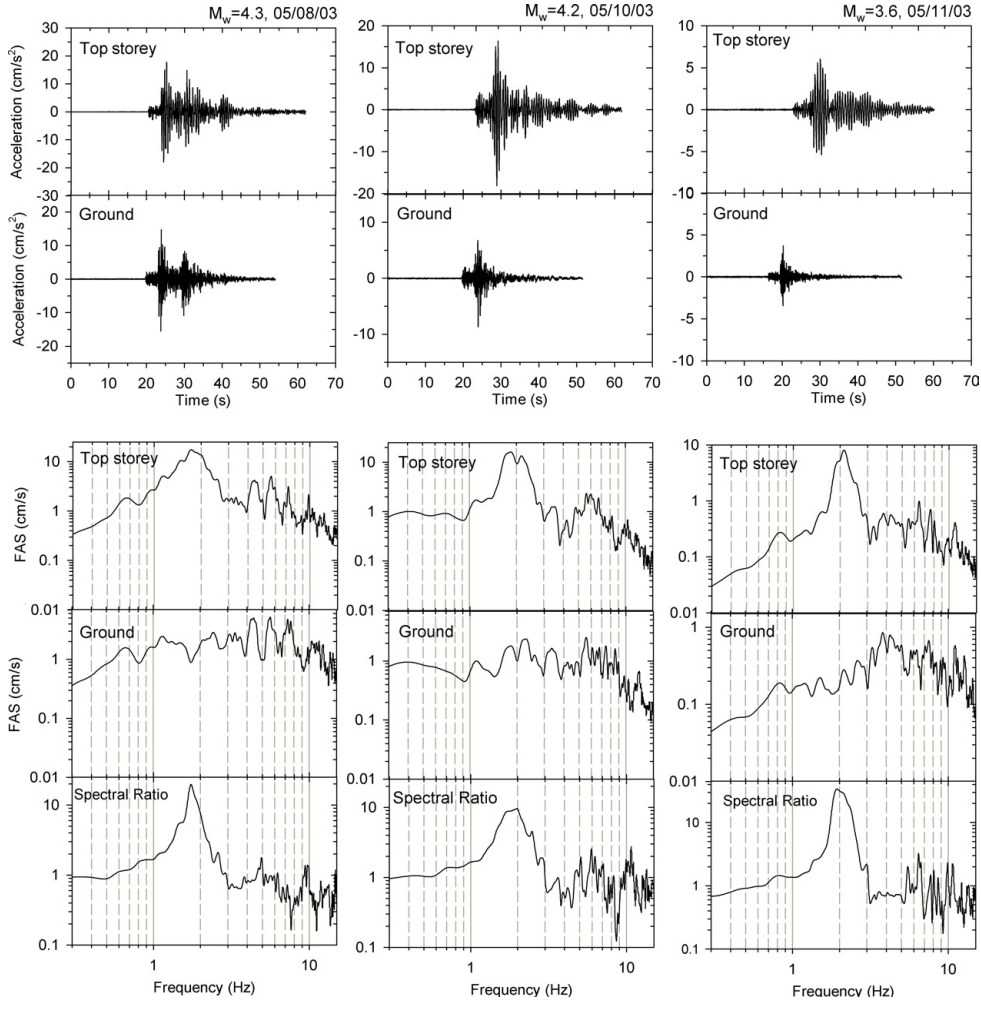

Fig. 12. Acceleration time series, spectra and spectral ratios for N10E component ground and top storey records during 3 aftershock events. The transducers at the top and ground level have the same polarity. The spectral curves represent the smoothed data by Parzen's lag window with a bandwidth of 0.2 Hz. The smoothing process did not destroy any important peaks in the data. (The ordinates of the figures do not have the same scale.)

the ground motion. These peaks are not nearly as clear in the spectra for the other two aftershocks (although the **M**3.6 aftershock seems to have a peak at 7.5 Hz). This is not surprising: Because of earthquake-to-earthquake variability at a single site, the spectral peaks may not always be in the same places or show up at all. The similar peak at 7.5 Hz for two of the aftershocks shown in Fig. 12, as well as the average of 59 aftershocks (Fig. 11) suggests that that peak may be due to a common effect on all records. If a site effect, then the somewhat lower frequency of the mainshock spectral peak could be due to a shift to lower frequencies due to

the decreasing rigidity resulting from nonlinear soil response to the strong shaking. Other peaks may be due to source or path effects.

In sum, we think a combination of factors contributed to the large ground motions, with various effects playing more-or-less important roles for various ranges of ground-motion frequencies. These effects include pedestal response, building pounding, radiation pattern, rupture directivity, and site response. Among these possibilities, the site response seems to be more reasonable than the others.

6. Engineering Aspects of the Ground Motion Data

The engineering aspects of the Bingöl record are discussed by describing some important strong ground motion parameters of engineering concern. The elastic/inelastic spectral responses affected by the high, narrow-band spectral amplitude at 6.5 Hz (0.15 seconds) and the pulse signal in the N10E component follow this discussion.

6.1. *Strong ground motion parameters*

Table 1 lists some of the important strong ground motion parameters of the Bingöl station data. The effective peak acceleration (EPA) of the horizontal components has values that are approximately 85% of their corresponding peak ground acceleration values. This ground-motion parameter has no real merit for explaining the complex seismological features of the ground motions but it is still used among some engineers to obtain the smoothed design spectrum of a given ground acceleration. The Arias intensity (AI) of the N10E component is almost 2.5 times larger than that of the E10S component. The significant duration value based on the time interval between 5% and 95% of the total AI [Trifunac and Brady, 1975] suggests that the strong motion duration (t_{sd}) of the N10E component is approximately 4.5 seconds. This interval is approximately 7 seconds in the E10S component. The considerable amount of energy that was imparted by the N10E component to structures within a very short interval of time is the indication of potential destructive power of the N10E component with respect to the other horizontal component. We believe that the high energy in this component is due mostly to the 4 second pulse signal period

Table 1. Strong ground motion parameters of the Bingöl station record.

Comp.	PGA	PGV	PGD	EPA	AI	t_{sd}	$\frac{\text{PGV}}{\text{PGA}}$
N10E	535.3	36.1	26.6	441.2	196.6	4.58	0.067
E10S	271.5	22.1	10.1	253.1	82.0	6.90	0.081
UP	463.3	13.6	8.2	199.2	80.60	6.21	0.029

• PGA, PGV and PGD units are cm/s^2, cm/s, and cm, respectively.
• EPA, and AI units are cm/s^2 and cm/s, respectively. (EPA is the average 5% damped spectral acceleration over the period range 0.1 s to 0.5 s divided by 2.5.)
• t_{sd} and PGV/PGA are in seconds.

that can be observed in the displacement plots shown in Fig. 5. The average AI of the horizontal components for the Bingöl record is 139.3 cm/s. There is a significant difference between this value and the value based on a recent ground-motion prediction equation [Travasarou *et al.*, 2003] that suggests median values of 55 cm/s to 34.5 cm/s for a magnitude 6.4 earthquake with closest site-to-fault rupture distances varying between 5 km and 10 km and site conditions similar to the Bingöl station.

In general, the peak velocity to peak acceleration (PGV/PGA) ratio is used for defining the frequency content of a ground motion or to characterise the structural damage capacity of ground motion. The PGV/PGA ratios of N10E and E10S are 0.067 and 0.081 seconds, respectively. The lower PGV/PGA ratio in the N10E (horizontal component with a significant pulse) could be attributed to the high PGA value as discussed in the preceding section.

6.2. *Construction of site specific design spectra from the observed ground motion*

The large spectral amplification of the N10E mainshock component shown in Figs. 8 and 11 is also pronounced in the pseudo-spectral acceleration (PSA) and leads to severe overestimation of design spectra when the procedure in the FEMA-356 document [BSSC, 2000] is blindly followed. We show this in Fig. 13. The method takes the short-period design response acceleration ($PSA_{0.2}$) as the response acceleration obtained from the site-specific spectrum at the period of 0.2 seconds unless the peak response acceleration at any period is less than 90% of this value. This value constitutes the design spectrum value for the constant acceleration plateau. The design spectral values at the intermediate and long periods are computed by overlaying a smooth curve on the site-specific spectrum of the form $PSA_{1.0}/T$ ($PSA_{1.0}$ is the site-specific spectral acceleration at 1.0 seconds) such that the design spectral acceleration computed from this relation will not be less than 90% of the spectral acceleration values of the site specific spectrum. The corner period, T_s, between the constant acceleration plateau and the descending branch is $PSA_{1.0}/PSA_{0.2}$. The large PSA amplification of the N10E component at approximately 0.15 seconds exhibits a high-amplitude, very narrow plateau, producing a large envelope of the design spectrum for almost all periods considered in Fig. 13. The overestimation in the spectral displacements (SD) is more pronounced. The exact elastic spectrum and the constructed design curve of the N10E component are also compared by plotting PSA against SD (with period as an implicit variable, $T = 2\pi(\mathrm{SD}/\mathrm{PSA})^{1/2}$). This spectrum is called the acceleration-displacement response spectrum (ADRS) and it forms the basis for the simplified nonlinear static procedure described in ATC-40 [ATC, 1996]. The plot confirms that the difference between the exact and smoothed curves is more pronounced in the short-period region in terms of PSA and in the long-period region in terms of SD. The design spectrum based on the ATC-40 procedure may lead to erroneous performance estimates of structures if this

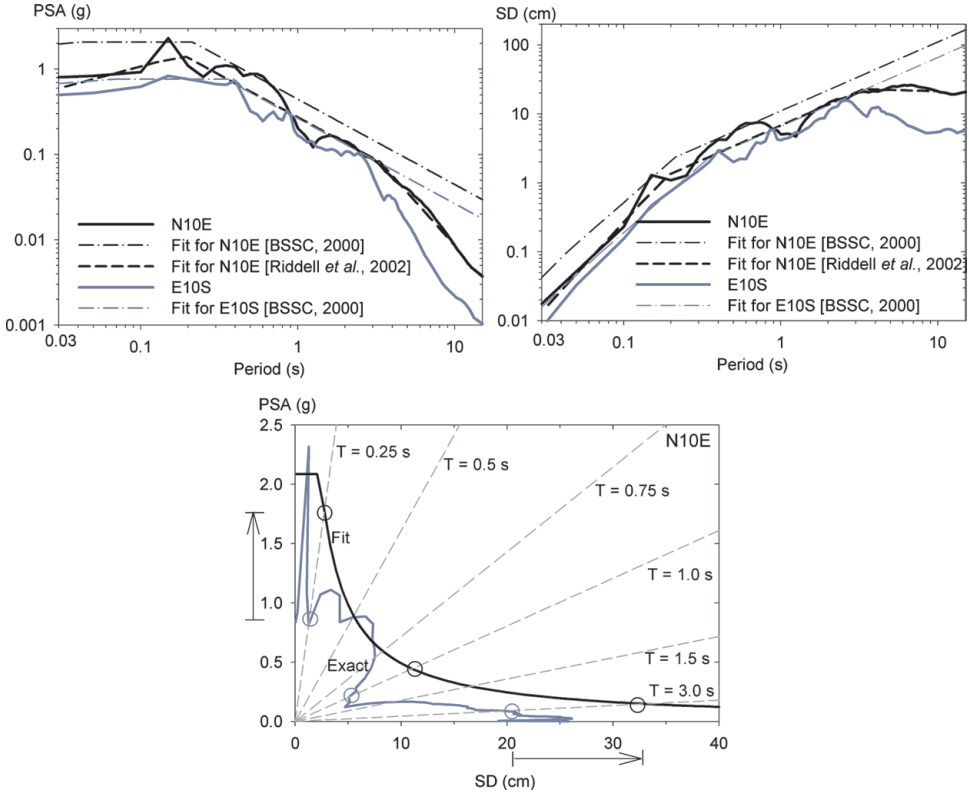

Fig. 13. 5% damped elastic spectra for the horizontal components. The frames display the PSA and SD of site specific design spectra for the horizontal components computed by the procedure described in FEMA-356 [BSSC, 2000]. We also computed the design spectrum of N10E component by Riddell *et al.* [2002] procedure to compare the results of FEMA method. The lower frame shows the exact and site specific design spectrum of FEMA in the acceleration-displacement response spectrum format. The difference in the spectral accelerations is more pronounced in the short period range. As the period shifts towards longer periods the spectral displacements computed from the actual spectra and design spectra fall apart from each other significantly for the FEMA procedure.

smoothed curve is used as the starting point of the method. The difference between the corner periods computed for the N10E and E10S components is also significantly different for this case. The corner period for E10S is 0.36 seconds whereas this value is 0.21 seconds in the N10E component. The value of 0.21 seconds is not representative of the design spectra for NEHRP B site classes [BSSC, 2000].

We also constructed a design spectrum for the N10E component following the procedure described by Riddell *et al.* [2002] in order to confirm that the observations highlighted above are specific to the FEMA-356 method. The Riddell *et al.* procedure defines acceleration-, velocity-, and displacement-sensitive regions on the spectrum, and fits a series of straight lines in order to idealise the jagged spectrum as a smooth curve. The results of the fitting process are also presented in Fig. 13.

The corner period of 0.196 seconds is similar to the one computed by the FEMA-356 procedure. The smoothed PSA values of this method are not as high as the spectral values computed by the FEMA-356 procedure. The descending branch at long periods shows a better fit to the observed spectrum but it inadequately envelopes the spectral values between 0.3 and 1.0 seconds. The spectral displacements show a very good match with the actual demand. This simple case shows that smoothing procedures suggest different ground demands due to the PSA amplification at 0.15 seconds.

6.3. *Inelastic spectral response*

Inelastic spectral displacements (SD_i) are realistic parameters for defining the deformation demand of ground motions on structural systems. Figure 14 shows the amplification of SD_i with respect to elastic spectral displacement SD_e for elasto-plastic systems whose lateral capacities are defined by strength reduction factors R. This factor is simply the strength required to maintain the system elastic normalised

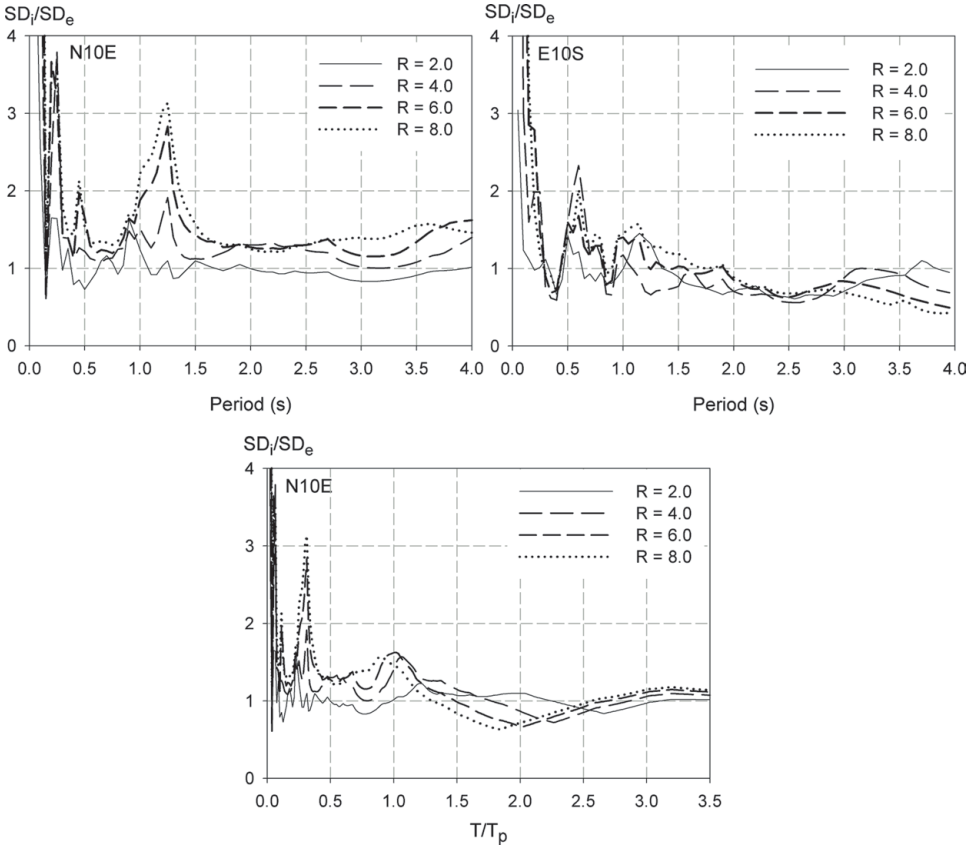

Fig. 14. Constant strength spectral displacement amplifications.

by the yield strength of the oscillator. Inelastic displacement spectra computed for a given R show the inelastic deformation demand of the ground motion for that lateral strength capacity. Figure 14 also shows that the N10E component has a very local SD_i/SD_e amplification at about 1.25 seconds. The Fourier spectrum of this component presented earlier in Fig. 11 shows a significant trough within this period range. This can be an interesting demonstration for the importance of excitation frequency content in nonlinear structural behaviour.

In agreement with the fundamentals of nonlinear dynamic behaviour of structures, the SD_i/SD_e ratio is sensitive to changes in R, with a significant amplification at short periods. In most accelerograms, independent from the strength reduction factor, the SD_i/SD_e ratios are equal to or less than one for periods larger than 1.25 seconds validating the equal displacement rule. (The equal displacement is an empirical rule stating that, on average, for long period ranges the maximum deformation of the inelastic system is equal to the maximum deformation of the elastic system.) The general trend in the SD_i/SD_e ratio computed for the E10S component follows this trend. However, the same figure also shows that the N10E component yields SD_i/SD_e values significantly larger than one even for periods longer than 3.0 seconds. This is the influence of the pulse signal that has a period of 4.0 seconds as shown in the displacement traces of Fig. 5. In fact, if the same spectral curves were drawn for periods normalised with respect to the pulse period, we would have obtained a clearer picture for the effect of pulse signal on the inelastic deformation demands. This is done in the lower frame presented in Fig. 14. These curves show that the equal displacement rule is valid for periods of vibration approximately 10 to 20% larger than the pulse period. This feature of pulse signals should be a serious concern for the building performance assessment methods.

7. Summary and Conclusions

This study has presented an evaluation of the Bingöl station accelerogram recorded during the 01 May 2003 **M**6.4 Bingöl earthquake. The earthquake occurred on a very complex faulting system that is inside one of the most seismically active zones in Turkey. The peak ground values of $0.55\,g$ and 36 cm/s are among the largest to be recorded to date in Turkey. The interpretations in this paper depend on the well-documented Bingöl station record and they are somewhat conjectural. We have used other pertinent data when available, such as the motions from 59 aftershocks recorded at the same site as the mainshock, and records from three aftershocks recorded in the top floor of the large building. In addition, we used various simulations of the ground motion in our interpretation.

The comparisons with ground motion prediction equations of similar recordings suggest that the motions on the N10E Bingöl record are unusually large, particularly for periods less than about 1.0 second. Our analyses showed that the large, narrow-band peak observed in the spectral amplitude at approximately 6.5 Hz is the main controlling parameter of the anomalous high value for the PGA. Among several

explanations for this narrow-band amplification, local site response seems to be the most reasonable. The computations on the actual and simulated mainshock data recorded from the same station and the amplifications based on our shear-wave velocity model encourage this finding. Other possibilities such as building pounding, pedestal resonance, directivity, or interaction of source corner frequency and local attenuation are also possible explanations for the high-amplitude peak.

The ground motion is strongly polarised in the north-south direction, which is not the fault normal direction for any of the hypothesised locations of the fault rupture surface. The polarisation and the significant ramp between P- and S-waves in the ground motion are interesting features of the Bingöl seismogram that is consistent with simulated motions for a slip distribution concentrated near the hypocentre.

The high, narrow-band peak that is observed in the Fourier spectrum amplitude is also dominant in PSA and causes an unrealistic design spectrum when procedures based on spectral accelerations at particular periods are directly implemented. The application of such a design spectrum to a displacement based design procedure might cause inappropriate decisions on the structural performance. The long period pulse signal in the N10E component causes enhanced inelastic deformation demands with respect to elastic demand for very long periods.

Acknowledgements

We thank the Earthquake Research Division of the General Directorate of Disaster Affairs in Ankara for providing the accelerograms used in the analyses. Numerous individuals contributed to this article, including Ulubey Çeken and Mustafa Gürbüz for the shear-wave velocity model, Dr. Nuretdin Kaymakçı for discussions of the local geology, Dominik Lang for various discussions and for reminding us of the paper by Wen *et al.* [2001], the NSF team for information regarding the orientation of the sensor, Rob Graves for providing the results of his ground-motion simulations, and Xu Li for providing an electronic version of his presentation at the 2004 annual meeting of the Seismological Society of America. We also express our sincere gratitude to Charles Mueller and Chris Stephens and two anonymous reviewers for their contributions leading to improvements in the article.

References

Abrahamson, N. A. [2000] "Effects of rupture directivity on probabilistic seismic hazard analysis," *Proc. of the Sixth International Conference on Seismic Zonation*, Earthquake Engineering Research Institute, Palm Springs, California, CD-Rom Paper No. 50.

Abrahamson, N. A. and Silva, W. J. [1997] "Empirical response spectral attenuation relations for shallow crustal earthquakes," *Seismological Research Letters* **68**(1), 94–127.

Akkar, S. and Gülkan, P. [2002] "A critical examination of near-field accelerograms from the Sea of Marmara region earthquakes," *Bulletin of the Seismological Society of America* **92**(1), 428–447.

Ambraseys, N. N. [1988] "Engineering seismology," *Earthquake Engineering and Structural Dynamics* **17**(1), 1–105.

Ambraseys, N. N. and Jackson, J. A. [1998] "Faulting associated with historical and recent earthquakes in the Eastern Mediterranean region," *Geophysics J. Int.* **33**, 390–406.

Ambraseys, N. N. and Douglas, J. [2003] "Near-field horizontal and vertical earthquake ground motions," *Soil Dynamics and Earthquake Engineering* **23**(1), 1–18.

Applied Technology Council (ATC) [1996] "Seismic evaluation and retrofit of concrete buildings," Report No. ATC-40, Redwood City, California.

Bakun, W. H. [1984] "Seismic moments, local magnitudes, and coda duration magnitudes for earthquakes in central California," *Bulletin of the Seismological Society of America* **74**(2), 439–458.

Boatwright, J. and Boore, D. M. [1982] "Analysis of the ground accelerations radiated by the 1980 Livermore Valley earthquakes for directivity and dynamic source characteristics," *Bulletin of the Seismological Society of America* **72**, 1843–1865.

Boore, D. M., Joyner, W. B. and Fumal, T. E. [1997] "Equations for estimating horizontal response spectra and peak acceleration from western North American earthquakes: A summary of recent work," *Seismological Research Letters* **68**(1), 128–153.

Boore, D. M. and Joyner, W. B. [1997] "Site amplifications for generic rock sites," *Bulletin of the Seismological Society of America* **87**(2), 327–341.

Boore, D. M. [2001] "Effect of baseline corrections on displacements and response spectra for several recordings of the 1999 Chi-Chi, Taiwan, earthquake," *Bulletin of the Seismological Society of America* **91**(5), 1199–1211.

Boore, D. M., Stephens, C. D. and Joyner, B. J. [2002] "Comments on baseline correction of digital strong-motion data: Examples from the 1999 Hector Mine, California, earthquake," *Bulletin of the Seismological Society of America* **92**(4), 1543–1560.

Boore, D. M. [2003] "Simulation of ground motion using the stochastic method," *Pure and Applied Geophysics* **160**(3), 635–676.

Boore, D. M. [2004] "Can site response be predicted?," *Journal of Earthquake Engineering* **8**(SI1), 1–41.

Boore, D. M. and Akkar, S. [2003] "Effect of causal and acausal filters on elastic and inelastic response spectra," *Earthquake Engineering and Structural Dynamics* **32**(11), 1729–1748.

Building Seismic Safety Council (BSSC) [2000] "Prestandard and commentary for the seismic rehabilitation of buildings," Report FEMA-356, Washington, DC.

Campbell, K. W. [1997] "Empirical near-source attenuation relationships for horizontal and vertical components of peak ground acceleration, peak ground velocity, and pseudo-absolute acceleration response spectra," *Seismological Research Letters* **68**(1), 154–179.

Campbell, K. W. [2000] Erratum to "Empirical near-source attenuation relationships for horizontal and vertical components of peak ground acceleration, peak ground velocity, and pseudo-absolute acceleration response spectra," by Kenneth W. Campbell, *Seismological Research Letters* **71**(1), 353–355.

Clough, R. and Penzien, J. [1993] *Dynamics of Structures 2nd Edition* (McGraw-Hill Inc., New York).

Converse, A. M. and Brady, A. G. [1992] "BAP — Basic strong-motion accelerogram processing software," Version 1.0, U.S. Geological Survey Open-File Report 92-296A, Menlo Park, California.

Çelebi, M. [2003] "Identification of site frequencies from building records," *Earthquake Spectra* **19**(1), 1–23.

Emre, Ö., Herece, E., Doğan, A., Parlak, O., Özaksoy, V., Çıplak, R. and Özalp, S. [2003] "The evaluation report on the May 1, 2003 Bingöl earthquake," Report No. 10585, The Directorate of Mine Survey and Research, Ankara, Turkey (in Turkish).

Gülkan, P. and Kalkan, E. [2002] "Attenuation modeling of recent earthquakes in Turkey," *Journal of Seismology* **6**, 397–409.

Howard, J. K., Tracy, C. A. and Burns, R. G. [2003] "Comparing observed and predicted directivity-amplified ground motion," *Eos Trans. AGU* **84**(46), *Fall Meet. Suppl.*, Abstract S52A-0120.

Iwan, W. D., Moser, M. A. and Peng, C.-Y. [1985] "Some observations on strong-motion earthquake measurement using a digital accelerograph," *Bulletin of the Seismological Society of America* **75**(5), 1225–1246.

Koçyiğit, A. and Kaymakçı, N. [2003] "The report of May 1, 2003 Sudüğünü (Sancak-Bingöl) earthquake," Tectonics and Earthquake Research Laboratory Report No. 14, Department of Geological Engineering, Middle East Technical University, Ankara, Turkey (in Turkish).

Lekidis, V. A., Karakostas, C. Z., Dimitriu, P. P., Margaris, B. N., Kalogeras, I. and Theodulidis, N. [1999] "The Aigio (Greece) seismic sequence of June 1995: Seismological, strong motion data and effects of the earthquakes on structures," *Journal of Earthquake Engineering* **3**(3), 349–380.

Li, X., Kuleli, S. and Toksöz, M. N. [2004] "The rupture process of the 1 May 2003 Bingöl, Turkey M_w 6.4 Earthquake," (abstract), *Seismological Research Letters* **74**(2), 286.

Riddell, R., Garcia, J. E. and Garces, E. [2002] "Inelastic deformation response of SDOF systems subjected to earthquakes," *Earthquake Engineering and Structural Dynamics* **31**(3), 515–538.

Sadigh, K., Chang, C.-Y., Egan, J. A., Makdisi, F. and Youngs, R. R. [1997] "Attenuation relationships for shallow crustal earthquakes based on California strong motion data," *Seismological Research Letters* **68**(1), 180–189.

Seymen, I. and Aydın, A. [1972] "The Bingöl earthquake fault and its relationship with the North Anatolian fault," *MTA Journal* **79**, 1–8 (in Turkish).

Somerville, P. G., Smith, N. F., Graves, R. W. and Abrahamson, N. A. [1997] "Modification of empirical strong ground motion attenuation relations to include the amplitude and duration effects of rupture directivity," *Seismological Research Letters* **68**(1), 199–222.

Travasarou, T., Bray, J. D. and Abrahamson, N. A. [2003] "Empirical attenuation relationship for Arias Intensity," *Earthquake Engineering and Structural Dynamics* **32**(7), 1133–1155.

Trifunac, M. D. and Brady, A. G. [1975] "A study on the duration of strong earthquake ground motion," *Bulletin of the Seismological Society of America* **65**(3), 581–626.

Wen, K.-L., Peng, H.-Y., Tsai, Y.-B. and Chen, K.-C. [2001] "Why 1G was recorded at TCU129 site during the 1999 Chi-Chi, Taiwan earthquake," *Bulletin of the Seismological Society of America* **91**(5), 1255–1266.